

Accurate gravitational waveforms for binary-black-hole mergers with nearly extremal spins

Geoffrey Lovelace¹, Michael Boyle¹, Mark A. Scheel², Béla Szilágyi²

¹ Center for Radiophysics and Space Research, Cornell University, Ithaca, New York, 14853, USA

² Theoretical Astrophysics 350-17, California Institute of Technology, Pasadena, California 91125, USA

E-mail: geoffrey@astro.cornell.edu, boyle@astro.cornell.edu, scheel@tapir.caltech.edu, szilagy@tapir.caltech.edu

Abstract. Motivated by the possibility of observing gravitational waves from merging black holes whose spins are nearly extremal (i.e., 1 in dimensionless units), we present numerical waveforms from simulations of merging black holes with the highest spins simulated to date: (1) a 25.5-orbit inspiral, merger, and ringdown of two holes with equal masses and spins of magnitude 0.97 aligned with the orbital angular momentum; and (2) a previously reported 12.5-orbit inspiral, merger, and ringdown of two holes with equal masses and spins of magnitude 0.95 anti-aligned with the orbital angular momentum. First, we consider the horizon mass and spin evolution of the new aligned-spin simulation. During the inspiral, the horizon area and spin evolve in remarkably close agreement with Alvi’s analytic predictions, and the remnant hole’s final spin agrees reasonably well with several analytic predictions. We also find that the total energy emitted by a real astrophysical system with these parameters—almost all of which is radiated during the time included in this simulation—would be 10.952% of the initial mass at infinite separation. Second, we consider the gravitational waveforms for both simulations. After estimating their uncertainties, we compare the waveforms to several post-Newtonian approximants, finding significant disagreement well before merger, although the phase of the TaylorT4 approximant happens to agree remarkably well with the numerical prediction in the aligned-spin case. We find that the post-Newtonian waveforms have sufficient uncertainty that hybridized waveforms will require far longer numerical simulations (in the absence of improved post-Newtonian waveforms) for accurate parameter estimation of low-mass binary systems.

PACS numbers: 04.25.dg, 04.30.-w

1. Introduction

In the next decade, advanced ground-based detectors such as the advanced Laser Interferometer Gravitational-Wave Observatory (advanced LIGO) [1, 2], Virgo [3], and the Large-scale Cryogenic Gravitational-wave Telescope (LCGT) [4] are expected to directly observe gravitational waves for the first time; coalescing black holes are among the most important sources of gravitational waves for these detectors. Numerical predictions of binary-black-hole (BBH) waveforms are crucial tools for detecting

these waves: for example, the Numerical INjection Analysis (NINJA) project [5, 6] is testing gravitational-wave search pipelines using numerical BBH waveforms, and the Numerical-Relativity and Analytical-Relativity (NR-AR) project [7] is working to calibrate analytic template banks for gravitational-wave searches using numerical BBH waveforms. Numerical BBH waveforms are also important tools for parameter estimation [8, 9, 10, 11].

Beginning with Pretorius’s 2005 breakthrough [12], several groups have successfully completed numerical simulations of the inspiral, merger, and ringdown of BBHs in a variety of configurations (see references [13, 14] for recent reviews). Simulations of BBHs with merging holes whose spins are nearly extremal (i.e., ~ 1 in dimensionless units, the theoretical upper limit for stationary holes) are a challenging but potentially important case, since black holes with nearly extremal spin might exist [15, 16, 17, 18, 19, 20, 21, 22] and thus might be among the BBHs emitting gravitational waves. Almost all published BBH simulations to date start with initial data in which 3 of the 4 Einstein constraint equations are solved analytically using the solutions of Bowen and York [23, 24]; this choice of initial data limits the black-hole dimensionless spins to $\chi \lesssim 0.93$ [25, 26, 27]. Dain, Lousto, and Zlochower have closely approached this “Bowen-York limit” by evolving an equal-mass BBH with equal spins of magnitude $\chi = 0.924$ aligned with the orbital angular momentum [28]. Note that the Bowen-York limit is actually far from extremal in terms of the physical effects of the spin: for example, a black hole with spin $\chi = 0.93$ has only 59% of the rotational energy of an extremal hole of the same mass.

By using an alternative method to construct BBH initial data, one can surpass the Bowen-York limit. In reference [29], three of us (Lovelace, Scheel, and Szilágyi) constructed and evolved (through 12.5 orbits, merger, and ringdown) BBH initial data (based on a weighted superposition of two boosted, spinning Kerr-Schild black holes [30]) with equal masses and equal spins of magnitude $\chi = 0.94905$ anti-aligned with the orbital angular momentum. In this paper, we present a new BBH simulation (through 25.5 orbits of inspiral, merger, and ringdown) with spins of magnitude $\chi = 0.96950$ aligned with the orbital angular momentum. These simulations are the first to surpass the Bowen-York limit and contain the most nearly extremal black holes yet simulated, with the black holes with spin $\chi = 0.94905$ and $\chi = 0.96950$ having 65% and 72% as much rotational energy, respectively, as an extremal hole of the same mass.

In this paper, we consider the gravitational waveforms from these two simulations. We begin in Sec. 2 by summarizing the numerical methods we use to construct and evolve rapidly-spinning BBH initial data and also the methods used to extract and extrapolate the gravitational waveforms. In Sec. 3, we examine the horizon mass and spin evolution in the new $\chi = 0.96950$ simulation. Then, in Sec. 4.1, we examine the emitted gravitational waveforms and their accuracy. In Sec. 4.2, we compare the numerical waves to several post-Newtonian (pN) approximants. We conclude with a brief discussion of the implications of our results in Sec. 5.

2. Numerical methods

2.1. Initial data

To construct BBH initial data with rapid spins, we use the method of reference [30] and the references therein: we use a spectral elliptic solver [32] to solve the extended

Run	$ 1 - q $	χ_i^z	M_{ADM}/M	J_{ADM}^z/M^2	M_{final}/M	χ_{final}^z
$S_{++}^{0.97}$	$1. \times 10^{-8}$	+0.96950	0.992569	1.55877	0.89048	0.94496
	$\pm 6. \times 10^{-8}$	± 0.00001	± 0.000009	± 0.00003	± 0.00002	± 0.00001
$S_{--}^{0.95}$	9.3×10^{-6}	-0.949047	0.99296	0.68404	0.968264	0.3757
	$\pm 4. \times 10^{-7}$	± 0.000009	± 0.00004	± 0.00006	± 0.000007	± 0.0002

Table 1. Some properties of the BBH simulations considered in this paper. The quantity q is the mass ratio, M is the sum of the holes’ Christodoulou masses, and hole i (where $i = A, B$) has dimensionless spin χ_i^z along the z axis (i.e., in the direction of the orbital angular momentum). Also listed are the Arnowitt-Deser-Misner (ADM) mass M_{ADM} and angular momentum J_{ADM}^z (e.g., Eqs. (25)–(26) of reference [30]) as well as the mass and spin of the final black hole. The quantities M , M_i , and χ_i^z are measured after the initial relaxation and junk radiation emission (at times $t = 1000M$ and $t = 500M$ for $S_{++}^{0.97}$ and $S_{--}^{0.95}$, respectively). Note that the mass M and spin χ_i^z are time-dependent; during the inspiral from infinite separation to the start of simulations $S_{++}^{0.97}$ and $S_{--}^{0.95}$, Alvi’s formulas [31] predict that the total mass M and spin χ_i^z would change by less than one part in 10^6 and by less than one part in 10^4 , respectively. The ADM quantities M_{ADM} and J_{ADM} are evaluated at $t = 0$, and M_{final} and χ_{final}^z are measured at the final time of the simulation. All uncertainties are estimated as the difference between the quantity at highest and second-highest resolution.

Run	d_0/M	\dot{r}_0/r_0	$\Omega_0 M$	e
$S_{++}^{0.97}$	15.362	0.00084325	0.013815	$6. \times 10^{-4} \pm 1. \times 10^{-4}$
$S_{--}^{0.95}$	15.368	-0.00071390	0.014507	$1. \times 10^{-3} \pm 1. \times 10^{-3}$

Table 2. The initial angular velocity Ω_0 , radial velocity \dot{r}_0/r_0 , and coordinate separation d_0 and the corresponding estimated orbital eccentricity e . The parameters d_0 , \dot{r}_0/r_0 , and Ω_0 are chosen when constructing the initial data; for simplicity, only the first five significant figures are shown.

conformal thin sandwich equations with quasi-equilibrium boundary conditions [33, 34, 35, 36, 37, 38]. We choose free data based on a superposition of two boosted, spinning Kerr-Schild black holes, tuning the freely specifiable parameters with a numerical root-finding algorithm based on Broyden’s method [39, 40] to obtain the desired masses and spins. We reduced the orbital eccentricity using the iterative technique of reference [41] which is based on fits of the orbital frequency.

We summarize the two configurations we consider in Tables 1 and 2.

2.2. Evolution

We evolve the initial data summarized in the Sec. 2.1 using the Spectral Einstein Code (SpEC) using the methods summarized in Sec. III of reference [29], which extend the techniques of reference [42] and the references therein to accommodate BBHs with spins above the Bowen-York limit. The evolution (but not the properties of the resulting gravitational waveform) of configuration $S_{--}^{0.95}$ was first reported in reference [29]; we present the evolution of configuration $S_{++}^{0.97}$ for the first time here. Full details of our methods will be given in a future paper; here, we merely summarize our method, highlighting some of the additional techniques necessary to merge $S_{++}^{0.97}$.

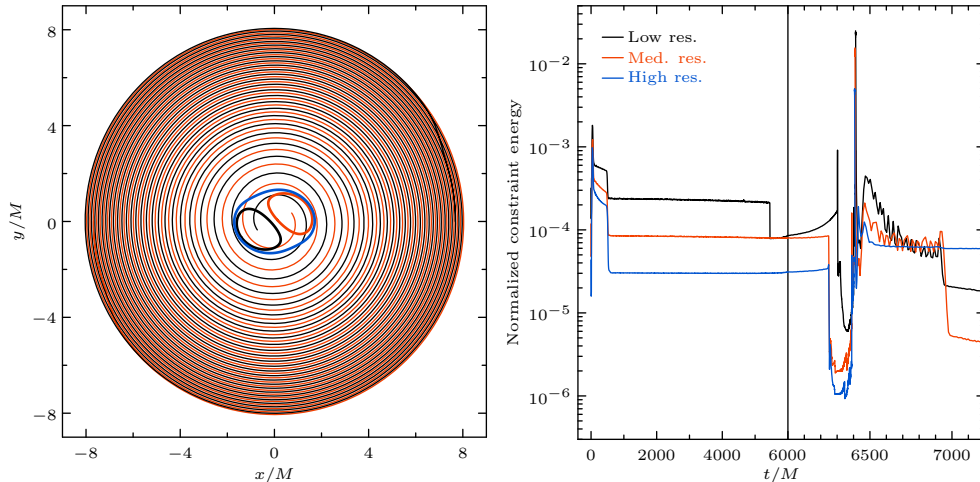


Figure 1. The trajectory and constraint violation in simulation $S_{++}^{0.97}$. *Left panel:* The trajectories of the centers of the individual apparent horizons. Also shown are the individual and common horizons at the final time at which the trajectories are shown. *Right panel:* For each resolution, the constraint violation (specifically, the normalized constraint energy defined in Eq. (71) of reference [43]) normalized over the entire computational domain. Also note that the horizontal scale changes at $t/M = 6000$.

As described in reference [29], we excise the singularities inside the black holes from our computational domain, using a time-dependent, adaptively adjusted coordinate mapping to keep the excision surfaces inside the horizons. Because we do not apply boundary conditions on the excision surface, the evolution is only well posed if the excision surface is a pure-outflow surface (i.e., if it has no incoming characteristic fields). During the inspiral, we enforce this condition by controlling the size of the excision surface such that it tracks the size of the apparent horizon; shortly before merger (i.e., during the final ~ 1 orbit of evolution $S_{--}^{0.95}$ and during the final ~ 3 orbits in the evolutions of $S_{++}^{0.97}$) we control the characteristic speeds directly by adjusting the velocity of the excision surface. During the final ~ 0.25 orbits before merger of $S_{--}^{0.95}$ and during the final ~ 3 orbits in $S_{++}^{0.97}$ we employed the spectral adaptive mesh refinement summarized in reference [29]. We also note that when evolving both $S_{--}^{0.95}$ and $S_{++}^{0.97}$, we smoothly change gauge conditions to the damped-harmonic condition described in reference [42] at the beginning of the evolution instead of shortly before merger.

Because the holes spend more time in a highly dynamical and distorted state, we find that merging $S_{++}^{0.97}$ requires that our coordinate mapping must track the apparent-horizon shapes more accurately (i.e., to a higher spherical-harmonic resolution ℓ). We also find that we must carefully fine-tune the characteristic speed control to balance two competing requirements: (1) that the excision surface have no incoming characteristic fields; and (2) that the excision surface remain inside the apparent horizon. Here, we do this fine-tuning manually in order to merge $S_{++}^{0.97}$; in the future, we plan to employ a method that handles any tuning automatically. Because the remnant hole also has a rapid spin [particularly just after it forms (figure 2)], we similarly control the horizon shape and characteristic speeds during the ringdown of

$S_{++}^{0.97}$ (with some manual fine-tuning).

To measure the characteristic speeds on the excision surface with sufficient accuracy near merger, just before merger in $S_{++}^{0.97}$ we adopt a computational domain where the individual apparent horizons lie within a thin, high-resolution spherical shell (instead of within a set of cylindrical subdomains, as evolution $S_{--}^{0.95}$ employed).

The right panel of figure 1 shows the numerical convergence of our method for the more demanding case $S_{++}^{0.97}$. The constraints initially grow, then drop as the initial burst of spurious gravitational radiation leaves the computational domain. The constraints then remain clearly convergent throughout the inspiral. Shortly before enabling spectral adaptive mesh refinement, we found it necessary to increase the resolution of the inner spheres in the low-resolution run in order to control adequately the characteristic speeds; this appears as a discontinuous drop in the low-resolution constraint energy. As the evolution approaches merger, the constraint violation grows in spite of the spectral adaptive mesh refinement. During ringdown, the constraints rapidly drop as the hole relaxes to its final state. As the radiation leaves the grid, the constraints drop sharply in the low and medium resolutions but not in the high resolution[‡].

Finally, we briefly note the computational cost of these two runs. Because the $S_{++}^{0.97}$ simulation involves higher spins, a very large orbital hangup effect (requiring twice as many orbits to merge from the same initial separation as the $S_{--}^{0.95}$ simulation), and a large amount of time in a regime where the spacetime is highly dynamical, the $S_{++}^{0.97}$ simulation turned out to be much more computationally expensive than the $S_{--}^{0.95}$ simulation. Specifically, the high-resolution simulation $S_{++}^{0.97}$ required $\approx 110,000$ cpu hours (≈ 120 days of wallclock time). For comparison, the high-resolution $S_{--}^{0.95}$ simulation required $\approx 20,000$ cpu hours (≈ 20 days of wallclock time).

2.3. Waveform extraction

We extract the gravitational waveform h using the Regge-Wheeler-Zerilli formalism [44, 45, 46, 47] on concentric spheres with radii from roughly $r = 100 M$ to $400 M$; we then extrapolate[§] the waveforms to infinite radius using the method of Boyle and Mroué [49] with polynomials of order $N = 4$. The waveforms are decomposed in the standard way [50] as modes $h_{\ell,m}$ of spin $s = -2$ spherical harmonics. We use these modes to define the amplitude and phase of the waveforms in the usual way:

$$A_{\ell,m}(\tau) = |r h_{\ell,m}(\tau)/M| \quad \phi_{\ell,m}(\tau) = \text{unwind} \{ \arg[h_{\ell,m}(\tau)] \} , \quad (1)$$

where the factor of r/M removes the radial dependence from $A_{\ell,m}$ and the unwind function removes discontinuities of 2π in the data caused by branch cuts [51]. We also

[‡] After a common horizon forms, our numerical simulation stops, interpolates onto a new computational domain with only a single excised region just inside the common horizon, and then continues using this new domain. Thus the numerical resolution used during the “plunge” (i.e., just before merger) is different than during the “ringdown” (i.e., just after merger). The lack of convergence at late times in figure 1 follows from differences in the medium and high plunge resolution. All 3 plunge resolutions required different fine-tuning in order to merge; we presume that these differences are responsible for the behavior visible in figure 1. We have verified that for the highest plunge resolution, the constraints converge with ringdown resolution, even at late times.

[§] We extract at finite radii and then extrapolate, since our computational domain only extends out to some finite radius. Extrapolation is meant to eliminate near-field effects and gauge dependence; to verify that the extrapolated waves do not retain any residual gauge dependence, the extrapolated waves could be compared with waveforms obtained using Cauchy Characteristic Extraction (CCE; see reference [48] and the references therein for details). In the future, we plan to compare CCE waveforms with the extrapolated waveforms presented in this paper.

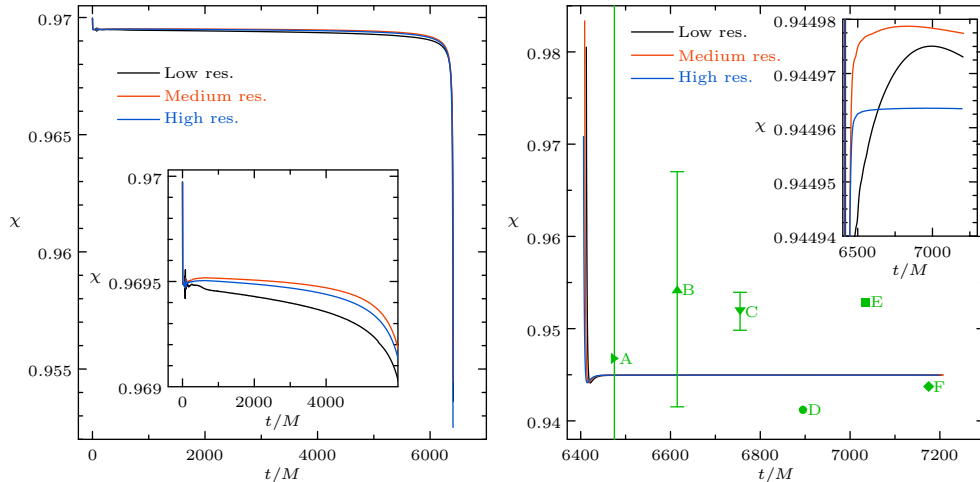


Figure 2. The spin evolution in simulation $S_{++}^{0.97}$. *Left panel:* The dimensionless spin χ as a function of time for one of the individual horizons. The inset zooms in on the spin during the inspiral. *Right panel:* The dimensionless spin χ of the common horizon as a function of time. Also shown, as individual data points with error bars where applicable, are the final spin predictions given by the analytic formulas in references [52] (“A”), [53] (“B”), [20] (“C”), [54] (“D”), [55] (“E”), and [56] (“F”). The inset zooms in on the final spin of the common horizon. The predictions are shown at different times simply for convenient separation.

use the frequency $\omega_{\ell,m}(\tau) = \partial_t \phi_{\ell,m}(\tau)$. We will occasionally drop the subscripts on these quantities, implicitly referring to $(\ell, m) = (2, 2)$.

3. Mass and spin evolution in the $S_{++}^{0.97}$ simulation

In figure 2, we show the dimensionless spin as a function of time for each resolution of the $S_{++}^{0.97}$ simulation. During the initial relaxation, the holes absorb energy, causing the dimensionless spin to quickly relax from $\chi = 0.9700$ at time $t = 0$ to $\chi = 0.9695$ at time $t = 1000M$.

Similarly to reference [28], we observe a very large orbital hangup [54, 57, 58] during the long inspiral: starting from the same initial coordinate separation (and thus at approximately the same initial orbital frequency), case $S_{++}^{0.97}$ requires more than twice as many orbits to merge as does case $S_{--}^{0.95}$ (compare the left panel of figure 1 and the top-left panel of figure 3 in reference [29]) and reaches roughly twice the orbital frequency. During this long inspiral, the spin remains above $\chi = 0.969$ during the first 21.5 orbits but then decreases near merger as the spin angular momentum is transformed into orbital angular momentum via tidal interactions.

The mechanism by which this transformation of angular momentum takes place has been described by numerous authors [59, 60, 61, 62, 63] including Alvi [31], who gave expressions for the rate at which energy and angular momentum would be transferred in comparable-mass binaries. In figure 3 we plot those rates as measured in the $S_{++}^{0.97}$ simulation and compare to those predicted by Alvi. Alvi’s expression uses the post-Newtonian velocity parameter v which we set to $v = (M\Omega)^{1/3}$, where Ω is the orbital angular frequency measured in the simulation. Though this comparison

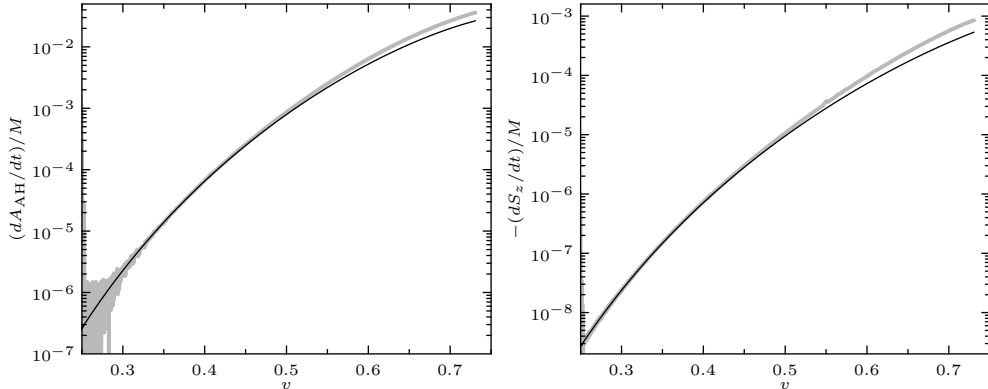


Figure 3. Change in irreducible mass and angular momentum of the horizons in the $S_{++}^{0.97}$ system compared with Alvi’s predictions [31]. *Left panel:* rate of change of irreducible (apparent-horizon) mass of the individual horizons. *Right panel:* rate of change of spin of the individual horizons. In each case, the noisier (thick gray) line represents data measured directly in the simulation, while the smoother (thin black) line is given by Alvi’s equation (11). The horizontal axis is parameterized by $v = (M\Omega)^{1/3}$, where Ω is the orbital frequency measured in the simulation. Note that $v \gtrsim 0.5$ corresponds to the last $\sim 40 M$ of time before merger.

is gauge dependent, we find very good agreement—within the numerical uncertainty until very late in the simulation. A similar comparison for the $S_{--}^{0.95}$ case is not as useful because the numerical uncertainties are far larger, though the result is consistent within the larger uncertainties. Note that this transfer of angular momentum is a 2.5-pN spin effect which is incorporated into the calculation of the pN waveforms in section 4.2.

When the common apparent horizon first forms, its spin is very nearly extremal but then quickly relaxes as the common horizon expands, eventually settling to a final spin $\chi_{\text{final}} = 0.94496 \pm 0.00001$, which is roughly consistent with the predictions of several analytic approximations (right panel of figure 2). The mass of the final hole is $M_{\text{final}}/M = 0.89048 \pm 0.00002$. Alvi’s formulas suggest that the mass would change by less than a part in 10^6 prior to the beginning of our simulation if the binary had inspiraled from infinite separation; therefore, a “real” binary would have radiated $E_{\text{rad}}/M = 1 - M_{\text{final}}/M = 10.952\% \pm 0.002\%$ of its initial mass ($= 12.299\% \pm 0.003\%$ of its final mass) throughout its entire inspiral, merger, and ringdown. This efficiency is comparable to that of a supernova ($\approx 15\%$ of the final core mass radiated; see, e.g., equation (18.1.1) of reference [64]) but corresponds to a larger total energy radiated (since the mass of a BBH is typically larger than the final core mass after a supernova). For comparison, the simulation in reference [65] implies that an equal-mass *nonspinning* binary system would radiate about 5% of its mass, while table 1 shows that the $S_{--}^{0.95}$ system radiates about 3.17% of its mass. When the merger occurs at a frequency in the sensitive band of a gravitational-wave detector, we can therefore expect that an aligned-spin system should have significantly larger SNR than a similar system with anti-aligned spins.

4. Gravitational waveforms and post-Newtonian comparisons

To compare two waveforms, A and B , we need to align them by fixing the arbitrary relative time and phase offsets. Here A and B may refer to two numerical waveforms with different resolutions or extrapolation orders, or A and B may refer to pN and numerical waveforms. Following reference [66], we align the waveforms by minimizing the difference in their phases over a certain range. Specifically, we minimize^{||} the quantity

$$\Xi(\Delta t, \Delta\phi) = \int_{t_1}^{t_2} [\phi_A(t) - \phi_B(t - \Delta t) - \Delta\phi]^2 dt . \quad (2)$$

Each mode of waveform B is then transformed as

$$h_{\ell,m}(t) \rightarrow h_{\ell,m}(t + \Delta t) e^{-im\Delta\phi/2} . \quad (3)$$

Note that ϕ refers to the phase of the $(\ell, m) = (2, 2)$ mode only; the values of Δt and $\Delta\phi$ are determined once, then each mode is transformed by this equation.

The optimal values of Δt and $\Delta\phi$ determined by minimizing equation (2) clearly depend on the range of integration (t_1, t_2) . We choose that range based on the frequencies of the waveform [10] so that $\omega(t_1) \approx 0.033$ and $\omega(t_2) \approx 0.038$.[¶] This gives us a common basis for comparison of the ranges used in the two cases of aligned and anti-aligned spins, despite the very different lengths of time over which they inspiral.

4.1. Waveform accuracy

We plot the amplitudes of the three dominant modes and the phase of the dominant $(\ell, m) = (2, 2)$ mode in the upper panels of figure 4 (for $S_{++}^{0.97}$) and figure 5 (for $S_{--}^{0.95}$). We also estimate the accuracy of the waveforms by measuring convergence with respect to increasing numerical resolution in the simulations and with respect to increasing order of the polynomial used for extrapolation to infinite radius. The relative amplitude convergence and phase convergence are plotted in the lower panels of the two figures.

The overall uncertainty estimate for a given quantity is the sum of the absolute values of the resolution convergence and the extrapolation convergence. That is, in the notation of the figures, we estimate

$$\text{Uncertainty} \approx |(\text{Med.}) - (\text{High})| + |(N = 4) - (N = 3)| . \quad (4)$$

For a waveform to be included in the NINJA-2 data set [5], the amplitude and phase of the $(2, 2)$ mode must be accurate at merger to within 5% and 0.5 rad, respectively. The $S_{--}^{0.95}$ case exceeds these requirements. The $S_{++}^{0.97}$ case, however, exceeds the amplitude requirement but does not meet the phase accuracy requirement. Through the time of merger, the amplitude uncertainty never exceeds 2%, but the phase uncertainty at the time of merger is 0.9 rad.

While the complete $S_{++}^{0.97}$ waveform does not meet the NINJA-2 *accuracy* requirement for phase, this simulation's 25.5 orbits far exceed the NINJA-2 *length* requirement of 5 orbits aligned with pN before a frequency of $M\omega = 0.075$. Indeed, if

^{||} For fixed Δt , the optimal $\Delta\phi$ can be obtained analytically, reducing the minimization to a one-dimensional problem. See reference [66] for details.

[¶] This range corresponds to $\delta\omega/\omega \approx 15\%$, which is somewhat larger than the 10% minimum recommended by MacDonald *et al.* [10]. We use a larger range to ensure that the alignment is not skewed by small oscillations in the data.

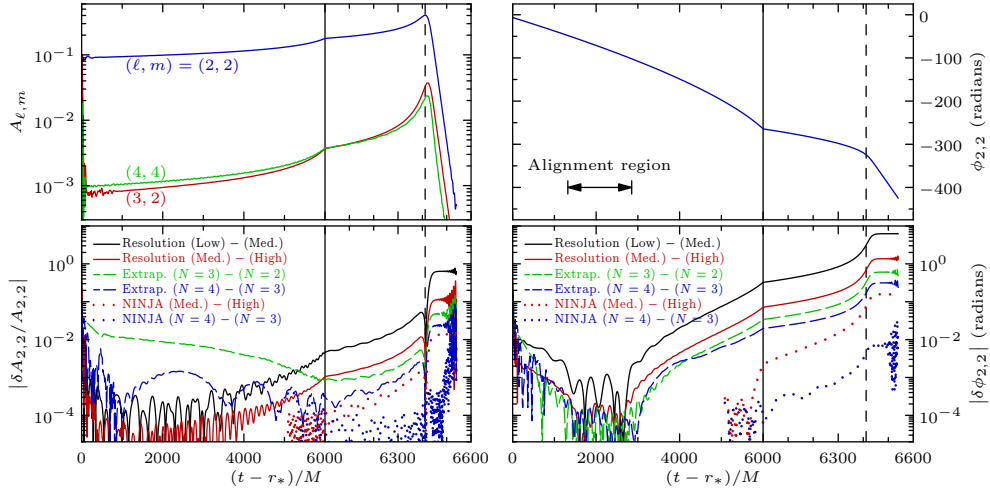


Figure 4. The extrapolated gravitational-wave amplitudes and phase for simulation $S_{++}^{0.97}$. *Left panel:* The dominant wave amplitudes $A_{2,2}$, $A_{3,2}$, and $A_{4,4}$ at high resolution (top) and relative differences $|\delta A_{2,2}/A_{2,2}|$ between resolutions or between extrapolation orders (bottom). *Right panel:* The phase ϕ at high resolution (top) and differences $|\delta\phi|$ between resolutions (bottom). When computing differences, the waveforms are aligned as in (2) between $(t-r_*)/M = 1322$ and $(t-r_*)/M = 2852$. The merger time $(t-r_*)/M = 6411$ is the time at which the $(2,2)$ amplitude is maximal, denoted by the vertical dashed lines. If the waveform were instead truncated to 5 orbits before merger (the NINJA-2 length requirement), the amplitude and phase errors would drop significantly (dotted lines). Note that the scale on the horizontal axis changes at $(t-r_*)/M = 6000$ in each plot for improved visibility of the merger and ringdown.

we omit the first $5000 M$ of the $S_{++}^{0.97}$ waveforms, the simulation still easily meets the length requirements. Evaluating the errors by aligning between the beginning of the shortened waveforms and $M\omega = 0.075$, the convergence measure improves by a factor of 10, and the simulation comfortably exceeds the NINJA-2 accuracy requirements with a phase uncertainty of 0.1 rad at the time of merger, as shown by the dotted lines in the lower panels of figure 4. Thus, we see that using accuracy requirements of this sort without regard to the length of the simulation actually creates a perverse incentive to produce *shorter* numerical waveforms, which *decreases* the accuracy of complete “hybridized” waveforms [11]. An exactly analogous situation occurs when the criteria require a particular match with respect to a detector noise curve but do not stipulate a mass at which that match should be measured; again, the incentive is to produce shorter waveforms.

4.2. Comparison with post-Newtonian approximations

The post-Newtonian waveform is constructed in two steps: (1) computation of the orbital phase of the binary; and (2) computation of the amplitude of the waveform using that phase. For nonspinning systems, the formulas needed for those computations have been calculated to 3.0-pN order beyond the leading order in amplitude and 3.5-pN beyond leading order in phase. Additional spin-orbit and spin-

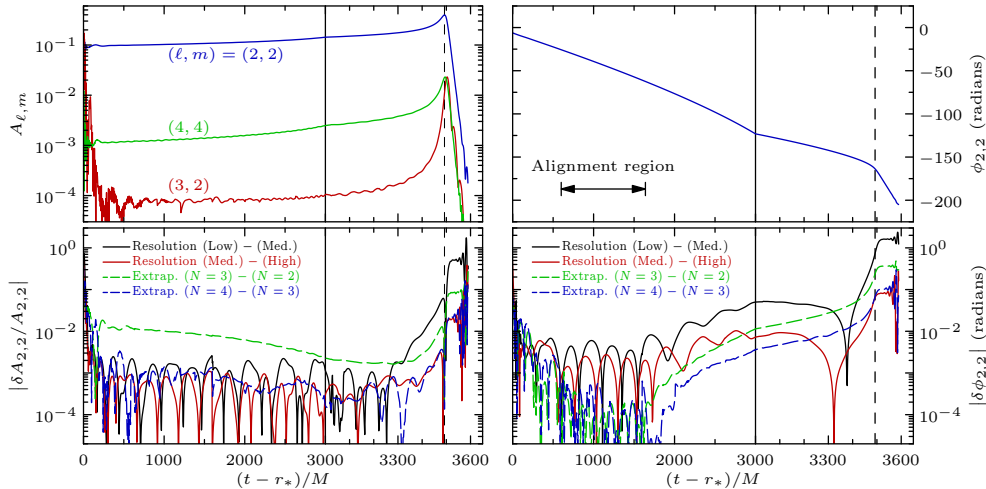


Figure 5. The extrapolated gravitational-wave amplitudes and phase as in figure 4 but for the $S_{--}^{0.95}$ simulation. Here, alignment is performed between $(t - r_*)/M = 600$ and $(t - r_*)/M = 1640$. This simulation is much shorter than the aligned case (about half the number of orbits), even though both simulations start at the same coordinate separation and consequently at roughly the same frequency. Here the anti-aligned spins cause the holes to merge more quickly than an analogous non-spinning binary, whereas in case $S_{++}^{0.97}$ the binary experiences a large orbital hangup. Note that the scale on the horizontal axis changes at $(t - r_*)/M = 3000$ in each plot for improved visibility of the merger and ringdown.

spin terms are available to 3.0-pN order in phase and amplitude,⁺ though not all of these have yet been expressed in a useful form for generating waveforms. We use the expressions given in appendix 1 of [50] for the flux, orbital energy, and tidal heating; and the expressions given in equation (9.4) of reference [68] and appendix 2 of reference [50] for the waveform amplitudes. The sole addition we make is the inclusion of a recently published spin-orbit contribution to the flux. In [50], equation (A.13) should be supplemented by adding a term [67] as

$$\mathcal{F}(v) \rightarrow \mathcal{F}(v) + \frac{32}{5} v^{10} \eta^2 \left\{ v^6 \left[-\frac{\pi}{6} \left(65 \delta \chi_a + (65 - 68 \nu) \chi_s \right) \right] \right\}. \quad (5)$$

Though formally high in order, this term is large enough in magnitude (for the spins we present) to dominate the next-to-leading-order spin contribution to the flux during most of the simulations, dominating even the leading-order term several hundred M before merger.

The orbital phase is computed using an energy-balance equation incorporating the rate of change of orbital energy and the loss of that energy in the form of tidal heating and the gravitational-wave energy flux \mathcal{F} . Various methods exist—referred to as the TaylorT1, T2, T3, and T4 approximants [69, 70, 51]—for integrating these equations, all of which should be equivalent to the pN order available, in the sense that they differ only by higher-order pN terms. This suggests that all four approximants should agree with each other and with the numerical waveform, within the uncertainty of the pN approximations. We have re-derived each of these approximants using the expressions described above and compared the results of each to the numerical waveforms.

⁺ See reference [67] and references therein.

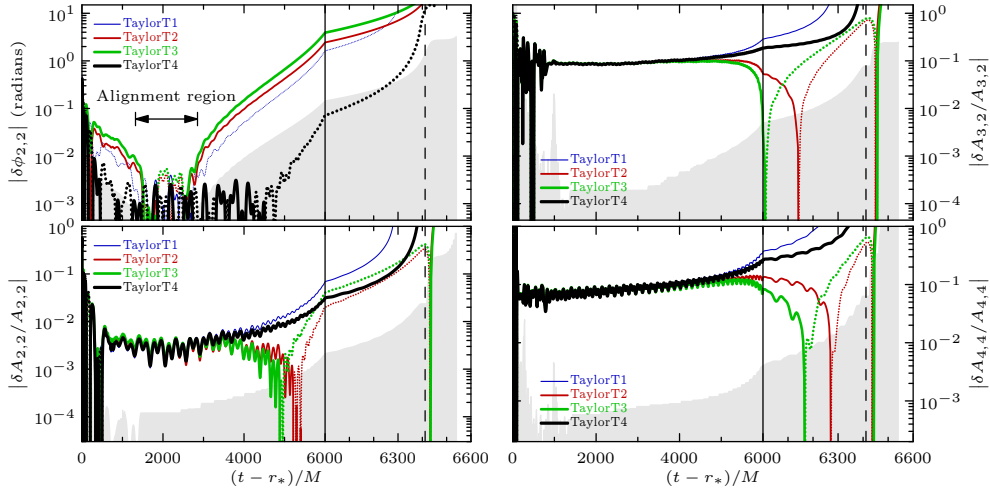


Figure 6. Comparison between numerical and pN data for the $S_{++}^{0.97}$ system for the four pN approximants. *Left panel:* Phase and relative amplitude errors for the dominant $(\ell, m) = (2, 2)$ mode. *Right panel:* Relative amplitude errors for the next two leading modes, $(\ell, m) = (3, 2)$ and $(4, 4)$. In all plots, the shaded gray region denotes our estimate for the numerical uncertainty, described by equation 4. Finely dotted portions of the graphs indicate negative errors; the pN quantity is larger than the numerical quantity in these regions. Note that the scale on the horizontal axis changes at $(t - r_*)/M = 6000$ in each plot for improved visibility of the merger and ringdown.

Figures 6 and 7 show the pN comparisons for $S_{++}^{0.97}$ and $S_{--}^{0.95}$, respectively. Only the phase of the $(2, 2)$ mode is shown, because the phases of other modes are integer multiples of this to a good degree of accuracy. The gray region in the background of each plot shows our uncertainty estimate for the numerical data of the given quantity, given by equation (4), and made to be a non-decreasing function of time after the beginning of the alignment region.

One remarkable feature is that the TaylorT4 approximant captures the phase surprisingly well for the $S_{++}^{0.97}$ system (black line in the top left plot of figure 6); it agrees with the numerical data within the uncertainty for roughly $3400M$ after the end of the alignment region (in which it is *forced* to agree with the numerical data). This brings it within $200M$ of the merger. Contrast that agreement with the other approximants, which disagree with the numerical data immediately after (or even before) the end of the alignment region.

Of course, this agreement of TaylorT4 is presumably pure coincidence, as all approximants agree with each other within the uncertainty of the pN approximations. The same coincidence was found in the equal-mass nonspinning case [51], but has been shown not to carry over to systems with other parameters (see, e.g., [58]). Indeed, looking at the $S_{--}^{0.95}$ system (figure 7), we see that the TaylorT4 approximant is actually the second worst in that case—the sole worse approximant being TaylorT3, which has *decreasing* orbital frequency starting just before the simulation, and is thus an especially poor description of the waveform.* We also point out that the $S_{++}^{0.97}$ system

* To be more precise, the TaylorT3 approximant expresses the orbital frequency of the binary as a function of the pN time to coalescence by inverting a power series (which is used directly for

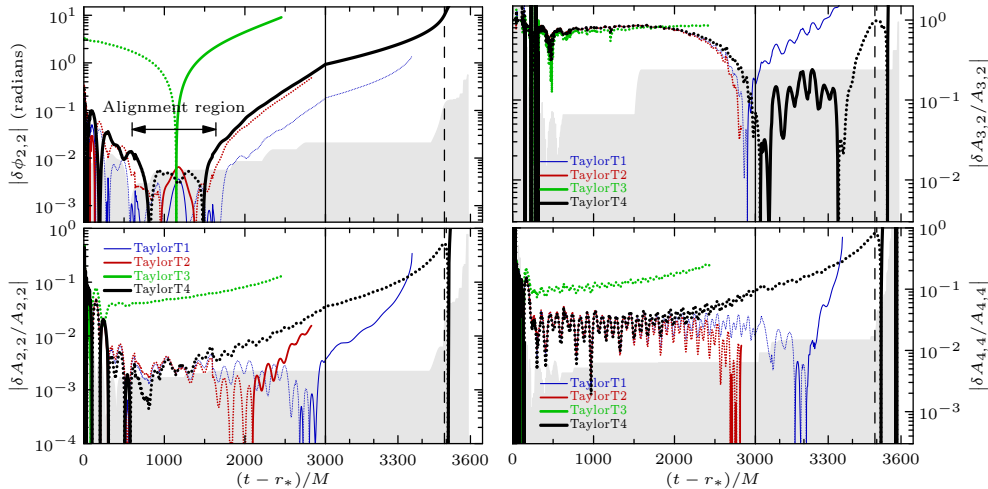


Figure 7. Comparison between numerical and pN data as in figure 6 but for the $S_{--}^{0.95}$ system. Note the difference in horizontal scale compared to figure 6. Note that the scale on the horizontal axis changes at $(t - r_*)/M = 3000$ in each plot for improved visibility of the merger and ringdown.

inspirals for roughly twice as long as the $S_{--}^{0.95}$ system and reaches nearly twice the frequency, making the phase coherence of TaylorT4 all the more surprising.

The figures also show the accuracy of the pN approximations for the amplitudes of the three dominant modes. In each case, the amplitude of the $(\ell, m) = (2, 2)$ mode is the most accurate, becoming worse for higher modes. This is to be expected, as the relative pN order to which the amplitudes are known decreases with increasing ℓ . In particular, the $(2, 2)$ mode is known to relative 3-pN order, while the $(3, 2)$ and $(4, 4)$ modes are only known to relative 2-pN order. Nonetheless, because of their far smaller magnitude, these higher-order modes actually have comparable *absolute* accuracy.

The $(3, 2)$ mode is particularly interesting. In the $S_{++}^{0.97}$ case, its amplitude is comparable to that of the $(4, 4)$ mode. However, in the $S_{--}^{0.95}$ case, the $(3, 2)$ mode is far smaller until the merger. For most of the inspiral, the pN amplitude error is very large—being off by roughly 80%. Again, however, this error is relative; the pN approximation correctly predicts that the amplitude should be quite small in this case, because of a cancellation between the leading-order nonspinning and spinning components of the amplitude.

Finally, we note that both waveforms can be hybridized to pN waveforms at frequencies of $M\omega \approx 0.035$, though these hybrids are not necessarily accurate enough to be useful in parameter estimation for detector-data analysis. As in reference [11], we can estimate the error in any hybrid by measuring the mismatch [71, 72, 73] between each pair of hybrids formed with the various approximants TaylorT1–T4; the error estimate is the maximum such mismatch. Using the Advanced LIGO high-power noise curve with no detuning [74] to do this measurement for the $S_{++}^{0.97}$ system, we find mismatches larger than 0.01 for total masses below roughly $40 M_\odot$. This

the TaylorT2 approximant). That frequency never reaches the initial frequency of our simulation; the frequency plot “turns over” before that point. This is not unusual behavior for TaylorT3. For example, even in the nonspinning case, similar behavior is seen for mass ratio 10 : 1. Evidently, the series-inversion procedure is not particularly accurate.

means that, for any detected ($\text{SNR} \gtrsim 8$) system with a lower mass, the uncertainty in these hybrids would be larger than the statistical uncertainty due to noise in the detector [75, 76]. For stronger signals or lower masses, more accurate pN waveforms and/or longer numerical simulations would be needed. For the $S_{--}^{0.95}$ case, a similar comparison would lead us to conclude that the hybrid is completely uncertain because of the bad behavior of the TaylorT3 approximant. If, on the other hand, we exclude that approximant as anomalously bad, we find that the hybrids are only accurate enough for parameter estimation above roughly $60 M_{\odot}$. Still, it is possible that such hybrids would be accurate enough for *detection* purposes [77].

5. Conclusion

The simulations discussed in this paper contain the most nearly extremal BBHs simulated to date. In our spin 0.97 simulation, we have found remarkably good agreement between the horizons’ mass and spin evolutions and Alvi’s analytic predictions, but we have found only moderately good agreement between the remnant hole’s final spin and several analytic formulas, which suggests that these analytic formulas could be improved significantly using a set aligned and anti-aligned nearly-extremal BBH simulations.

We have found that the waveform from the 12.5-orbit anti-aligned case $S_{--}^{0.95}$ exceeds the NINJA-2 accuracy requirements, while the waveform from the 25.5-orbit aligned case $S_{++}^{0.97}$ exceeds the NINJA-2 amplitude requirement but (because it is so long) fails to meet the NINJA-2 phase requirement (although it does meet the phase requirement easily if truncated to 5 orbits, the NINJA-2 length requirement).

These results demonstrate the feasibility of applying waveforms from numerical simulations to gravitational-wave data analysis efforts when the holes have nearly extremal spins—a case previously inaccessible numerically but relevant astrophysically, given the evidence that nearly extremal black holes could exist. For example, waveforms such as those considered in this paper could be used in calibrating analytic template banks used for gravitational-wave detection searches. To pursue this goal, we plan to apply our methods for evolving nearly extremal BBHs to a large variety of BBH configurations, including unequal masses and spin precession.

We have compared our numerical waveforms to several pN approximants, finding that the pN and numerical waveforms disagree at times well before merger. We also find that the pN approximants disagree with one another, indicating a large uncertainty in the pN approximations which leads to a large uncertainty in the resulting hybridized waveforms. Extracting the BBH parameters from detector data for systems with nearly extremal spins will require far longer numerical simulations, far more accurate pN waveforms, or a combination of the two. In the absence of improved pN waveforms, however, this implies that parameter estimation when the holes have nearly extremal spins could prove quite challenging, since the longer numerical simulations that would be necessary will come at high computational cost.

Acknowledgments

We are pleased to thank Nick Taylor for a gauge modification that allows us to use the non-smooth maps of reference [42] throughout our evolutions and Larry Kidder, Robert Owen, Harald Pfeiffer, Saul Teukolsky, and Kip Thorne for helpful discussions. This work was supported in part by grants from the Sherman Fairchild Foundation to

Caltech and Cornell and from the Brinson Foundation to Caltech; by NSF Grants No. PHY-0601459, No. PHY-1068881, and No. PHY-1005655 at Caltech; by NASA Grant No. NNX09AF97G at Caltech; by NSF Grants No. PHY-0969111 and No. PHY-1005426 at Cornell; and by NASA Grant No. NNX09AF96G at Cornell. The numerical computations presented in this paper were performed primarily on the Caltech compute cluster ZWICKY, which was funded by the Sherman Fairchild Foundation and the NSF MRI-R² grant No. PHY-0960291 to Caltech. Some computations were also performed on the GPC supercomputer at the SciNet HPC Consortium; SciNet is funded by: the Canada Foundation for Innovation under the auspices of Compute Canada; the Government of Ontario; Ontario Research Fund - Research Excellence; and the University of Toronto. Some computations were performed in part using TeraGrid resources provided by NCSA's Ranger cluster under Grant No. TG-PHY990007N.

References

- [1] Barry C. Barish and Rainer Weiss. LIGO and the detection of gravitational waves. *Phys. Today*, 52(10):44–50, Oct 1999.
- [2] Daniel Sigg and the LIGO Scientific Collaboration. Status of the LIGO detectors. *Class. Quantum Grav.*, 25(11):114041, 2008.
- [3] F. Acernese et al. Virgo status. *Class. Quantum Grav.*, 25(18):184001, 2008.
- [4] K Kuroda and the LCGT Collaboration. Status of LCGT. *Class. Quantum Grav.*, 27(8):084004, 2010.
- [5] The NINJA collaboration. www.ninja-project.org.
- [6] B. Aylott, J. G. Baker, W. D. Boggs, M. Boyle, P. R. Brady, D. A. Brown, B. Brügmann, L. T. Buchman, A. Buonanno, L. Cadonati, J. Camp, M. Campanelli, J. Centrella, S. Chatterji, N. Christensen, T. Chu, P. Diener, N. Dorband, Z. B. Etienne, J. Faber, S. Fairhurst, B. Farr, S. Fischetti, G. Guidi, L. M. Goggin, M. Hannam, F. Herrmann, I. Hinder, S. Husa, V. Kalogera, D. Keppel, L. E. Kidder, B. J. Kelly, B. Krishnan, P. Laguna, C. O. Lousto, I. Mandel, P. Marronetti, R. Matzner, S. T. McWilliams, K. D. Matthews, R. A. Mercer, S. R. P. Mohapatra, A. H. Mroué, H. Nakano, E. Ochsner, Y. Pan, L. Pekowsky, H. P. Pfeiffer, D. Pollney, F. Pretorius, V. Raymond, C. Reisswig, L. Rezzolla, O. Rinne, C. Robinson, C. Röver, L. Santamaría, B. Sathyaprakash, M. A. Scheel, E. Schnetter, J. Seiler, S. L. Shapiro, D. Shoemaker, U. Sperhake, A. Stroeer, R. Sturani, W. Tichy, Y. T. Liu, M. van der Sluys, J. R. van Meter, R. Vaulin, A. Vecchio, J. Veitch, A. Viceré, J. T. Whelan, and Y. Zlochower. Testing gravitational-wave searches with numerical relativity waveforms: Results from the first Numerical INjection Analysis (NINJA) project. *Class. Quantum Grav.*, 26(16):165008, 2009.
- [7] The numerical relativity and analytical relativity (NRAR) collaboration. <https://www.ninja-project.org/doku.php?id=nrar:home>.
- [8] M. Hannam, S. Husa, F. Ohme, and P. Ajith. Length requirements for numerical-relativity waveforms. *Phys. Rev. D*, 82(12):124052, 2010.
- [9] T. Damour, A. Nagar, and M. Trias. Accuracy and effectualness of closed-form, frequency-domain waveforms for nonspinning black hole binaries. *Phys. Rev. D*, 83(2):024006, 2011.
- [10] Ilana MacDonald, Samaya Nissanke, and Harald P. Pfeiffer. Suitability of post-Newtonian/numerical-relativity hybrid waveforms for gravitational wave detectors. *Class. Quantum Grav.*, 28(13):134002, July 2011.
- [11] Michael Boyle. Uncertainty in hybrid gravitational waveforms: Optimizing initial orbital frequencies for binary black-hole simulations. *Phys. Rev. D*, 84, September 2011.
- [12] Frans Pretorius. Evolution of binary black-hole spacetimes. *Phys. Rev. Lett.*, 95(12):121101, 2005.
- [13] J. M. Centrella, J. G. Baker, B. J. Kelly, and J. R. van Meter. Black-hole binaries, gravitational waves, and numerical relativity. *Rev. Mod. Phys.*, 82:3069, 2010.
- [14] Sean T. McWilliams. The Status of Black-Hole Binary Merger Simulations with Numerical Relativity. *Class. Quant. Grav.*, 28:134001, 2011.
- [15] Kip S. Thorne. Disk-accretion onto a black hole. ii. evolution of the hole. *Astrophys. J.*, 191:507, 1974.

- [16] Charles F Gammie, Stuart L Shapiro, and Jonathan C McKinney. Black hole spin evolution. *Astrophys. J.*, 602:312, 2004.
- [17] Stuart L Shapiro. Spin, accretion, and the cosmological growth of supermassive black holes. *Astrophys. J.*, 620:59, 2005.
- [18] Jeffrey E McClintock, Rebecca Shafee, Ramesh Narayan, Ronald A Remillard, Shane W Davis, and Li-Xin Li. The spin of the near-extreme Kerr black hole GRS 1915+105. *Astrophys. J.*, 652:518, 2006.
- [19] Jian-Min Wang, Yan-Mei Chen, Luis C Ho, and Ross J McLure. Evidence for rapidly spinning black holes in quasars. *Astrophys. J.*, 642:L111, 2006.
- [20] Luciano Rezzolla et al. Spin Diagrams for Equal-Mass Black-Hole Binaries with Aligned Spins. *Astrophys. J.*, 679:1422–1426, 2008.
- [21] Michael Kesden. Can binary mergers produce maximally spinning black holes? *Phys. Rev. D*, 78:084030, 2008.
- [22] Michael Kesden, Guglielmo Lockhart, and E. Sterl Phinney. Maximum black-hole spin from quasi-circular binary mergers. *Phys. Rev. D*, 82:124045, 2010.
- [23] Jeffrey M. Bowen. General form for the longitudinal momentum of a spherically symmetric source. *Gen. Relativ. Gravit.*, 11(3):227–231, 1979.
- [24] Jeffrey M. Bowen and James W. York, Jr. Time-asymmetric initial data for black holes and black-hole collisions. *Phys. Rev. D*, 21(8):2047–2056, 1980.
- [25] Gregory B. Cook and James W. York, Jr. Apparent horizons for boosted or spinning black holes. *Phys. Rev. D*, 41(4):1077–1085, 1990.
- [26] Sergio Dain, Carlos O. Lousto, and Ryoji Takahashi. New conformally flat initial data for spinning black holes. *Phys. Rev. D*, 65:104038, 2002.
- [27] Mark Hannam, Sacha Husa, and Niall. Ó Murchadha. Bowen-york trumpet data and black-hole simulations. *Phys. Rev. D*, 80:124007, 2009.
- [28] Sergio Dain, Carlos O Lousto, and Yosef Zlochower. Extra-large remnant recoil velocities and spins from near-extremal-Bowen–York-spin black-hole binaries. *Phys. Rev. D*, 78:024039, 2008.
- [29] Geoffrey Lovelace, Mark A. Scheel, and Bela Szilagyi. Simulating merging binary black holes with nearly extremal spins. *Phys. Rev. D*, 83:024010, 2011.
- [30] Geoffrey Lovelace, Robert Owen, Harald P. Pfeiffer, and Tony Chu. Binary-black-hole initial data with nearly-extremal spins. *Phys. Rev. D*, 78:084017, 2008.
- [31] Kashif Alvi. Energy and angular momentum flow into a black hole in a binary. *Phys. Rev. D*, 64(10):104020, Oct 2001.
- [32] H. P. Pfeiffer, L. E. Kidder, M. A. Scheel, and S. A. Teukolsky. A multidomain spectral method for solving elliptic equations. *Comput. Phys. Commun.*, 152:253–273, 2003.
- [33] James W. York. Conformal “thin-sandwich” data for the initial-value problem of general relativity. *Phys. Rev. Lett.*, 82(7):1350–1353, Feb 1999.
- [34] Gregory B. Cook. Corotating and irrotational binary black holes in quasicircular orbits. *Phys. Rev. D*, 65(8):084003, Mar 2002.
- [35] Gregory B. Cook and Harald P. Pfeiffer. Excision boundary conditions for black-hole initial data. *Phys. Rev. D*, 70(10):104016, Nov 2004.
- [36] Matthew Caudill, Greg B. Cook, Jason D. Grigsby, and Harald P. Pfeiffer. Circular orbits and spin in black-hole initial data. *Phys. Rev. D*, 74(6):064011, 2006.
- [37] Eric Gourgoulhon, Philippe Grandclément, and Silvano Bonazzola. Binary black holes in circular orbits. I. A global spacetime approach. *Phys. Rev. D*, 65:044020, 2002.
- [38] Philippe Grandclément, Eric Gourgoulhon, and Silvano Bonazzola. Binary black holes in circular orbits. II. numerical methods and first results. *Phys. Rev. D*, 65:044021, 2002.
- [39] C. G. Broyden. A class of methods for solving nonlinear simultaneous equations. *Math. Comp.*, 19(92):577–593, 1965.
- [40] W. H. Press, S. A. Teukolsky, W. T. Vetterling, and B. P. Flannery. *Numerical Recipes: The Art of Scientific Computing (3rd Ed.)*. Cambridge University Press, New York, 2007.
- [41] Alessandra Buonanno, Lawrence E. Kidder, Abdul H. Mroué, Harald P. Pfeiffer, and Andrea Taracchini. Reducing orbital eccentricity of precessing black-hole binaries. *Phys. Rev. D*, 83(10):104034, May 2011.
- [42] Bela Szilagyi, Lee Lindblom, and Mark A. Scheel. Simulations of Binary Black Hole Mergers Using Spectral Methods. *Phys. Rev. D*, 80:124010, 2009.
- [43] Lee Lindblom, Mark A. Scheel, Lawrence E. Kidder, Robert Owen, and Oliver Rinne. A new generalized harmonic evolution system. *Class. Quantum Grav.*, 23:S447–S462, 2006.
- [44] Tullio Regge and John A. Wheeler. Stability of a Schwarzschild singularity. *Phys. Rev.*, 108:1063–1069, 1957.

- [45] Frank J. Zerilli. Effective potential for even-parity ReggeWheeler gravitational perturbation equations. *Phys. Rev. Lett.*, 24:737–738, 1970.
- [46] Olivier Sarbach and Manuel Tiglio. Gauge-invariant perturbations of Schwarzschild black holes in horizon-penetrating coordinates. *Phys. Rev. D*, 64:084016, Sep 2001.
- [47] Oliver Rinne, Luisa T. Buchman, Mark A. Scheel, and Harald P. Pfeiffer. Implementation of higher-order absorbing boundary conditions for the Einstein equations. *Class. Quantum Grav.*, 26:075009, 2009.
- [48] M. C. Babiuc, B. Szilagyi, J. Winicour, and Y. Zlochower. A Characteristic Extraction Tool for Gravitational Waveforms. 2010.
- [49] Michael Boyle and Abdul H. Mroué. Extrapolating gravitational-wave data from numerical simulations. *Phys. Rev. D*, 80(12):124045–14, December 2009.
- [50] P. Ajith, Mike Boyle, Duncan A. Brown, Stephen Fairhurst, Mark Hannam, Ian Hinder, Sascha Husa, Badri Krishnan, R. A. Mercer, F. Ohme, C. D. Ott, J. S. Read, L. Santamaría, and J. T. Whelan. Data formats for numerical relativity, 2011. arXiv:0709.0093v3.
- [51] Michael Boyle, Duncan A. Brown, Lawrence E. Kidder, Abdul H. Mroué, Harald P. Pfeiffer, Mark A. Scheel, Gregory B. Cook, and Saul A. Teukolsky. High-accuracy comparison of numerical relativity simulations with post-Newtonian expansions. *Phys. Rev. D*, 76:124038, 2007.
- [52] W. Tichy and P. Marronetti. The final mass and spin of black hole mergers. *Phys. Rev. D*, 78:081501(R), 2008.
- [53] Enrico Barausse and Luciano Rezzolla. Predicting the direction of the final spin from the coalescence of two black holes. *Astrophys. J. Lett.*, 704:L40, 2009.
- [54] Manuela Campanelli, Carlos O. Lousto, and Yosef Zlochower. Gravitational radiation from spinning-black-hole binaries: The orbital hang up. *Phys. Rev. D*, 74:041501(R), 2006.
- [55] Alessandra Buonanno, Lawrence E. Kidder, and Luis Lehner. Estimating the final spin of a binary black hole coalescence. *Phys. Rev. D*, 77:026004, 2008.
- [56] L. Boyle and M. Kesden. The spin expansion for binary black hole merger: new predictions and future directions. *Phys. Rev. D*, 78:024017, 2008. arXiv:0712.2819 [astro-ph].
- [57] Luciano Rezzolla, Peter Diener, Ernst Nils Dorband, Denis Pollney, Christian Reisswig, et al. The Final spin from the coalescence of aligned-spin black-hole binaries. *Astrophys. J.*, 674:L29–L32, 2008.
- [58] Mark Hannam, Sascha Husa, Bernd Brügmann, and Achamveedu Gopakumar. Comparison between numerical-relativity and post-Newtonian waveforms from spinning binaries: the orbital hang-up case. *Phys. Rev. D*, 78:104007, 2008.
- [59] S. Teukolsky. Perturbations of a rotating black hole. fundamental equations for gravitational, electromagnetic, and neutrino-field perturbations. *Astrophys. J.*, 185, 1973.
- [60] James B. Hartle. Tidal Friction in Slowly Rotating Black Holes. *Phys. Rev.*, D8:1010–1024, 1973.
- [61] J Hartle. Tidal shapes and shifts on rotating black holes. *Phys. Rev. D*, 9:2749, 1974.
- [62] R.H. Price and K.S. Thorne. MEMBRANE VIEWPOINT ON BLACK HOLES: PROPERTIES AND EVOLUTION OF THE STRETCHED HORIZON. *Phys. Rev.*, D33:915–941, 1986.
- [63] Kip S. Thorne, Richard H. Price, and Douglas A. MacDonald. *Black Holes: The Membrane Paradigm*. Yale University Press, New Haven and London, first edition, 1986.
- [64] S. L. Shapiro and S. A. Teukolsky. *Black Holes, White Dwarfs and Neutron Stars*. Wiley, New York, 1983.
- [65] M. Scheel, M. Boyle, T. Chu, L. Kidder, K. Matthews and H. Pfeiffer. High-accuracy waveforms for binary black hole inspiral, merger, and ringdown. *Phys. Rev. D*, 79:024003, 2009.
- [66] Michael Boyle, Alessandra Buonanno, Lawrence E. Kidder, Abdul H. Mroué, Yi Pan, Harald P. Pfeiffer, and Mark A. Scheel. High-accuracy numerical simulation of black-hole binaries: Computation of the gravitational-wave energy flux and comparisons with post-Newtonian approximants. *Phys. Rev. D*, 78(12):104020, 2008.
- [67] Luc Blanchet, Alessandra Buonanno, and Guillaume Faye. Tail-induced spin-orbit effect in the gravitational radiation of compact binaries, April 2011.
- [68] Luc Blanchet, Guillaume Faye, Bala R. Iyer, and Siddhartha Sinha. The third post-Newtonian gravitational wave polarizations and associated spherical harmonic modes for inspiralling compact binaries in quasi-circular orbits. *Class. Quantum Grav.*, 25(16):165003, 2008.
- [69] Thibault Damour, Bala R. Iyer, and B. S. Sathyaprakash. Comparison of search templates for gravitational waves from binary inspiral. *Phys. Rev. D*, 63(4):044023, Jan 2001. Erratum: [78].
- [70] Alessandra Buonanno, Gregory B. Cook, and Frans Pretorius. Inspiral, merger, and ring-down of equal-mass black-hole binaries. *Phys. Rev. D*, 75(12):124018, 2007.

- [71] B. S. Sathyaprakash and S. V. Dhurandhar. Choice of filters for the detection of gravitational waves from coalescing binaries. *Phys. Rev. D*, 44(12):3819, December 1991.
- [72] R. Balasubramanian, B. S. Sathyaprakash, and S. V. Dhurandhar. Gravitational waves from coalescing binaries: Detection strategies and Monte Carlo estimation of parameters. *Phys. Rev. D*, 53(6):3033, March 1996.
- [73] Benjamin J. Owen. Search templates for gravitational waves from inspiraling binaries: Choice of template spacing. *Phys. Rev. D*, 53(12):6749, June 1996.
- [74] David Shoemaker. Advanced LIGO anticipated sensitivity curves, 2010. LIGO Document T0900288-v3.
- [75] E. E. Flanagan and S. A. Hughes. Measuring gravitational waves from binary black hole coalescences. I. Signal to noise for inspiral, merger, and ringdown. *Phys. Rev. D*, 57:4535, 1998.
- [76] Lee Lindblom, Benjamin J. Owen, and Duncan A. Brown. Model Waveform Accuracy Standards for Gravitational Wave Data Analysis. *Phys. Rev. D*, 78:124020, 2008.
- [77] Frank Ohme, Mark Hannam, and Sascha Husa. Reliability of complete gravitational waveform models for compact binary coalescences. *Phys. Rev. D*, 84:064029, September 2011.
- [78] Thibault Damour, Bala R. Iyer, and B. S. Sathyaprakash. Erratum: Comparison of search templates for gravitational waves from binary inspiral. *Phys. Rev. D*, 72(2):029902, 2005.